Supplementary Information

Built-In Electric Field Triggered Electron Transfer for Selective Singlet Oxygen Generation with Intrinsic Chemiluminescence

Wanli Zeng[a], Houjing Liu[a]*

[a]*Guizhou Key Laboratory of Macrocyclic and Supramolecular Chemistry, School of Chemistry and Chemical Engineering, Guizhou University, Guiyang 550025, China.*

**Corresponding Author. Email: hjliu3@gzu.edu.cn (Liu H.). Tel & Fax: +86-0851-8263906.*

Chemicals and Reagents. Phosphonitrilic chloride trimer (PCT), ascorbic acid (AA), p-benzoquinone (PBQ), methylene blue trihydrate (MB), europium nitrate ($Eu(NO_3)_3•6H_2O$), sodium sulfate (Na_2SO_4), 1,3-diphenylisobenzofuran (DPBF) and ammonium fluoride (NH_4F) were bought from Shanghai Titan Scientific Company (Shanghai, China). L-histidine (L-his), thiourea, and sodium hydroxide (NaOH) were purchased from National Group Chemical Reagent Company (Shanghai, China). Copper nitrate trihydrate ($Cu(NO_3)_2•3H_2O$) was procured from Kemel Reagent Company (Tianjin, China). Hexamethylene tetramine was bought form Jinshan Chemical Reagent Company (Chengdu, China). 2,2,6,6-tetramethylpiperidine (TEMP), 5,5-dimethyl-1-pyrroline N-oxide (DMPO) were purchased from Sinopharm Chemical Reagent Company (Shanghai, China). All chemical reagents were used at least of analytical grade and without further purification treatment. All solutions were prepared using ultrapure water (18.2 MΩ/cm), which was treated with a Mili-Q ultrapure instrument (Chengdu, China).

Instruments. Electron paramagnetic resonance (EPR) spectra were obtained by the Bruker E-500 instrument. Ultraviolet-visible diffuse-reflectance spectra was measured with an Ultraviolet-visible Near-Infrared spectrophotometer (UV-3600 PLUS, Japan). The morphology of the material was obtained by Transmission electron microscopy (TEM, Japan-JEOL-JEM 2100 F). X-ray diffraction (XRD) patterns of prepared materials were analyzed using an X-ray diffractometer (Rigaku Ultima IV, Japan) with

Cu target Kα rays. X-ray photoelectron spectroscopy (XPS) was tested on Thermo Scientific K-Alpha equipped with an Al Kα exciting. Fourier transform infrared (FT-IR) spectra was used to investigate the surface functional groups on a Nicolet iS10 FT-IR spectrometer (Thermo Scientific, America). Zeta potential measurements were performed with a Microelectrophoresis apparatus (JS94H2, China). Nuclear Magnetic Resonance Hydrogen Spectrum (^{1}H NMR) was recorded with JEOL-ECX 400MHz (Japan). CL spectra were carried on a Cary Eclipse fluorescence spectrophotometer (Varian, Inc., located in Palo Alto, USA).

CL experiment. All CL experiments were recorded by ultra-weak luminescence analyzer (BPCL-2-TGC, China). Detailly, for Eu-CuO@PNDs/Mn(VII)/SP system, a mixture of 200 μL Eu-CuO@PNDs (0.02 mg/mL) and 200 μL Mn(VII) (10^{-3} mol/L) solution was placed in a quartz cell. Then, 200 μL SP solution was injected from a container into the quartz cell to trigger CL reaction. Unless otherwise specified, the CL experiments were recorded with the voltage of the PMT (0.8 kV); an interval time of 0.01 s was used for data acquisition. Additionally, all CL measurements were performed in triplicate (n=3) to the date reliability.

CL quantum yield. The CL quantum yield (QY) value of the Eu-CuO@PNDs/Mn(VII)/SP system was determined by using the luminol-H_2O_2 system as the standard with a known CL QY of 1.14×10^{-2} E/mol at pH=11.6 (0.1 M K_2CO_3) according to the literature.[1] Briefly, the solution of Eu-CuO@PNDs (0.02 mg/mL)/Mn(VII) (1 mM) was placed in a tube, and then SP (0.2 μg/mL) was added to the solution. CL dynamic curves of the mixture were measured until the CL intensity reduced to 1% of the highest value. The voltage of PMT was 0.8 kV for the CL detection and signal acquisition time of the CL analyzer was set at 0.1 s in intensity mode. The same procedure was carried out with a mixture of luminol (1 μM, 100 μL, in 0.1 M K_2CO_3) and H_2O_2 (1 mM, 100 μL). The CL QY value of Eu-CuO@PNDs/Mn(VII)/SP system was relatively calculated from the integrated areas under curves according to the following equation:

$$\phi = \phi_{lum} \times \frac{I}{I_{lum}} \times \frac{n^2}{n_{lum}^2} \times \frac{[Luminol]}{[Eu - CuO@PNDs]}$$

ϕ is the quantum yield, where I is the total number of photons obtained by integration of CL dynamic curves under time until the CL intensity reduced to 1% of the highest value, n is the refractive index of solvent, and [Luminol] and [Eu-CuO@PNDs] were concentrations.

Note: The CL quantum yield (QY) values of the Eu-CuO@PNDs/Mn(VII)/SP system was 3.12×10^{-9} einsteins/mol.

$^1O_2$ quantification. The strongest UV-Vis absorption spectrum of DPBF is at 410 nm, which can react with $^1O_2$ in a 1:1 molar ratio. Therefore, DPBF can be used as $^1O_2$ trapping agent to quantify $^1O_2$ concentration.[2] During the CL experiment (0.02 mg Eu-CuO@PNDs, 1 mM Mn(VII) and 0.2 μg SP), 0.6 mL sample solution was taken immediately. And mixed with 1 mL DPBF solution and 1 mL ethanol to measure the UV-absorption intensity and calculate the $^1O_2$ generation concentration.

$$[^1O_2] = \frac{A_{0-A_t}}{\varepsilon b}$$

$[^1O_2]$ is the concentration of $^1O_2$, A_0 represents the absorbance at the initial time, and A_t is absorbance at 410 nm of DPBF immediately after mixing with Eu-CuO@PNDs/Mn(VII)/SP system, where ε is the molar extinction coefficient (3.0×10^{-4} M^{-1}/cm) at 410-415 nm, b is optical path length (1 cm).

Note: The $^1O_2$ concentrations for Eu-CuO@PNDs/Mn(VII)/SP and Mn(VII) solutions were 12.44 μM and 3.46 μM.

Electrochemical measurement. All electrochemical tests were characterized by CHI660E electrochemical workstation (Shanghai Chenhua, China) under the condition of a three-electrode system, with the Pt electrode and saturated calomel electrode (SCE) as a counter and reference electrode, respectively. The working electrode were bare or modified glassy carbon electrodes (GCE). To prepare modified-GCE, 20 mg catalyst powder was dispersed into 400 μL acetone solution containing 20 μL Nafion solution as the polymer binder. After that, the mixture was ultrasonicated for 30 min to form a

suspension. Subsequently, the suspension was dropped onto the GCE surface and kept dried. The linear sweep voltammetry (LSV), open circuit potential (OCP) and amperometric current-time (i-t) curves were all measured in a 0.1 M Na_2SO_4 solution.

Preparation of europium modified copper oxide (Eu-CuO). Eu-CuO was synthesized via hydrothermal method using $Cu(NO_3)_2•3H_2O$ and $Eu(NO_3)_3•6H_2O$ as precursors. Typically, 0.2 mmol $Cu(NO_3)_2•3H_2O$ and 2 mmol NH_4F were dispersed in 80 mL ultrapure water under constant agitation. Subsequently, 0.08 mmol hexamethylene tetramine and 0.4 mmol NaOH were added into the above mixture and stirred for 10 min to form blue uniform suspension at room temperature. Thirdly, 0.04 mmol $Eu(NO_3)_3•6H_2O$ solution was gradually added to the above suspension and stirred for 15 min. Next, the precursor suspensions were sealed into Teflon-lined reaction autoclaves and kept at 120 ℃ for 6 h. The final product of Eu-CuO was centrifuged at 10000 rpm for 10 min to collect the precipitates. For further purifying the Eu-CuO, the obtained precipitates were washed with ethanol and ultrapure water several times until neutral pH was achieved. Finally, the purified Eu-CuO material was vacuum dried at 50 °C for 12 h.

Preparation of nitrogen phosphide nanodots (PNDs). PNDs were synthesized based on previous literature.[3] Briefly, 20 mg PCT was mixed with 20 mL ethanol and transferred into Teflon-lined reaction autoclaves, and kept at 180 ℃ for 12 h. After cooling naturally, the obtained solution was filtered using a 0.22 μm syringe to separate the larger particles. The obtained filtrate was evaporated by spin evaporation at 50 °C to remove ethanol. Finally, the obtained sample was vacuumed at 50 °C for 6 h. The resulting product was dissolved in ultrapure water to obtain 1 mg/mL PNDs.

Preparation of Eu-CuO@PNDs heterojunction. The general synthetic procedure for Eu-Cu@PNDs heterojunction were described as follows. Firstly, the homogeneous dispersion of Eu-CuO was ultrasonically dispersed into ethanol. Then, 20 mL PCT solution was added into the suspension under continuous agitation. The mixture underwent hydrothermal treatment in sealed reactor maintained at 180 ℃ for 12 h. Post reaction purification was performed via membrane filtration using a 0.22 μm sterile

syringe filter to obtain the Eu-CuO@PNDs nanocomposite suspension. The target material was isolated through vacuum-assisted rotary evaporation at 50 °C followed by final desiccation in a vacuum oven at 50 °C for 10 h. The synthesis of the PNDs@Eu-CuO complex was similar to that of Eu-CuO@PNDs, wherein the PCT solution was replaced with the PNDs solution during the process, maintaining other experimental parameters unchanged.

Preparation of the PNDs/Eu-CuO heterojunction. For the synthesis of the PNDs/Eu-CuO heterojunction, 0.1 mmol $Cu(NO_3)_2 \cdot 3H_2O$ and 1 mmol NH_4F were dispersed in 40 mL ultrapure water under continuous agitation. Then, 0.04 mmol HMT and 0.2 mmol NaOH were added into the mixture under agitation, and stirred for 10 min to form blue uniform suspension at room temperature. Subsequently, 0.02 mmol $Eu(NO_3)_3 \cdot 6H_2O$ solution was gradually added into above suspension and stirred for 15 min. Finally, the PNDs solution was dropped into above suspension under stirring. The precursor suspensions were then sealed into Teflon-lined reaction autoclaves and kept at 120 ℃ for 6 h. The final product of PNDs/Eu-CuO was centrifuged at 10000 rpm for 10 min to collect the supernatant. The obtained filtrate was evaporated by spin evaporation at 90 °C and vacuum-dried at 50 °C for 12 h.

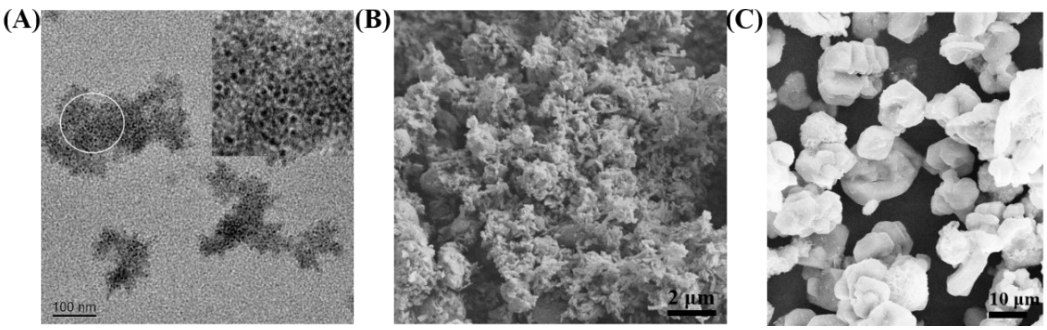

Figure S1. (A) TME image of Eu-CuO@PNDs. SEM images of (B) Eu-CuO and (C) Eu-CuO@PNDs.

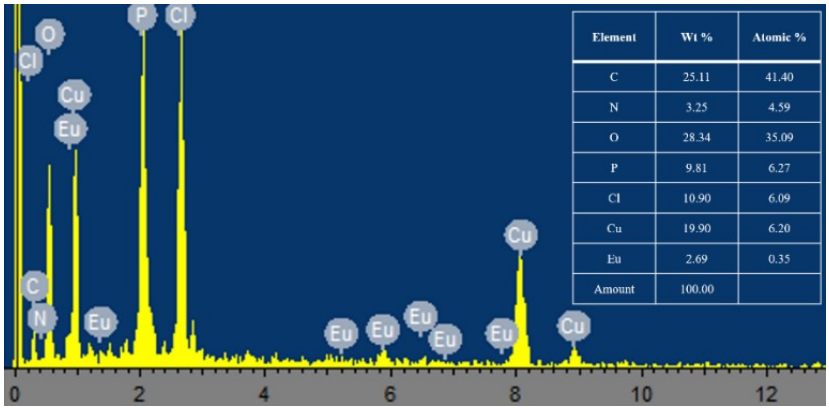

Element	Wt %	Atomic %
C	25.11	41.40
N	3.25	4.59
O	28.34	35.09
P	9.81	6.27
Cl	10.90	6.09
Cu	19.90	6.20
Eu	2.69	0.35
Amount	100.00	

Figure S2. EDS image of Eu-CuO@PNDs (inset: table of element composition).

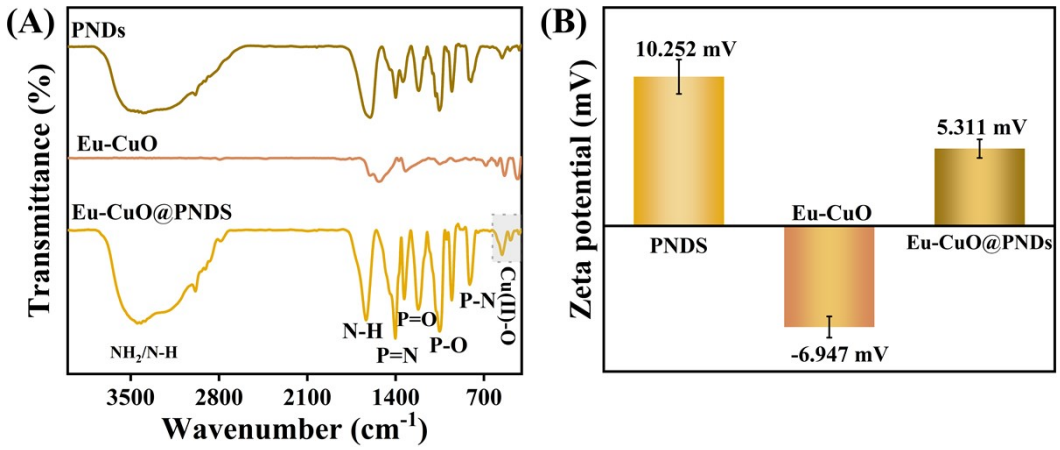

Figure S3. (A) FT-IR spectra and (B) Zeta potential of PNDs, Eu-CuO, and Eu-CuO@PNDs.

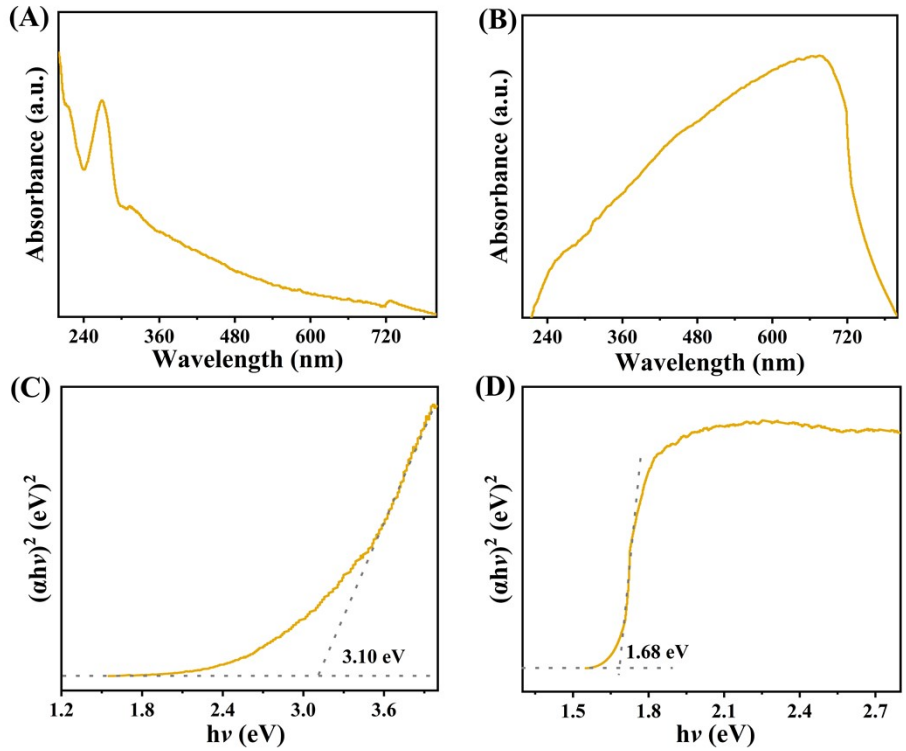

Figure S4. UV-vis DRS spectra of (A) PNDs and (B) Eu-CuO. The plots of $(\alpha h\nu)^2$ versus band gap energy ($h\nu$) of (C) PNDs and (D) Eu-CuO, respectively.

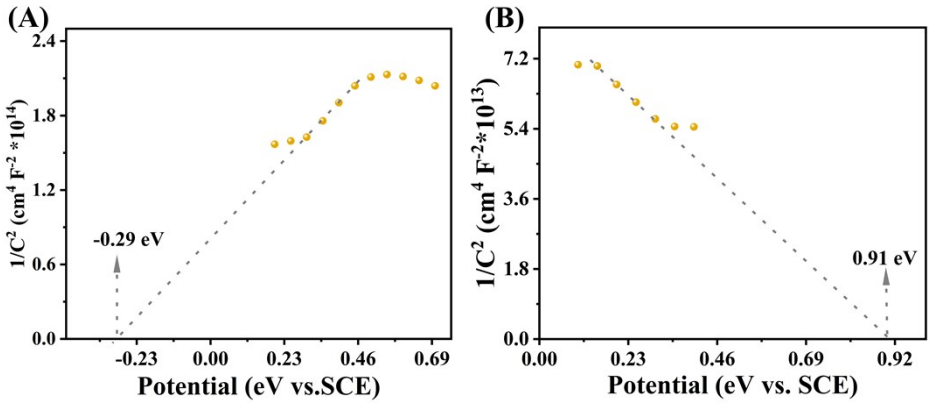

Figure S5. Mott-Schottky curves of (A) PNDs and (B) Eu-CuO.

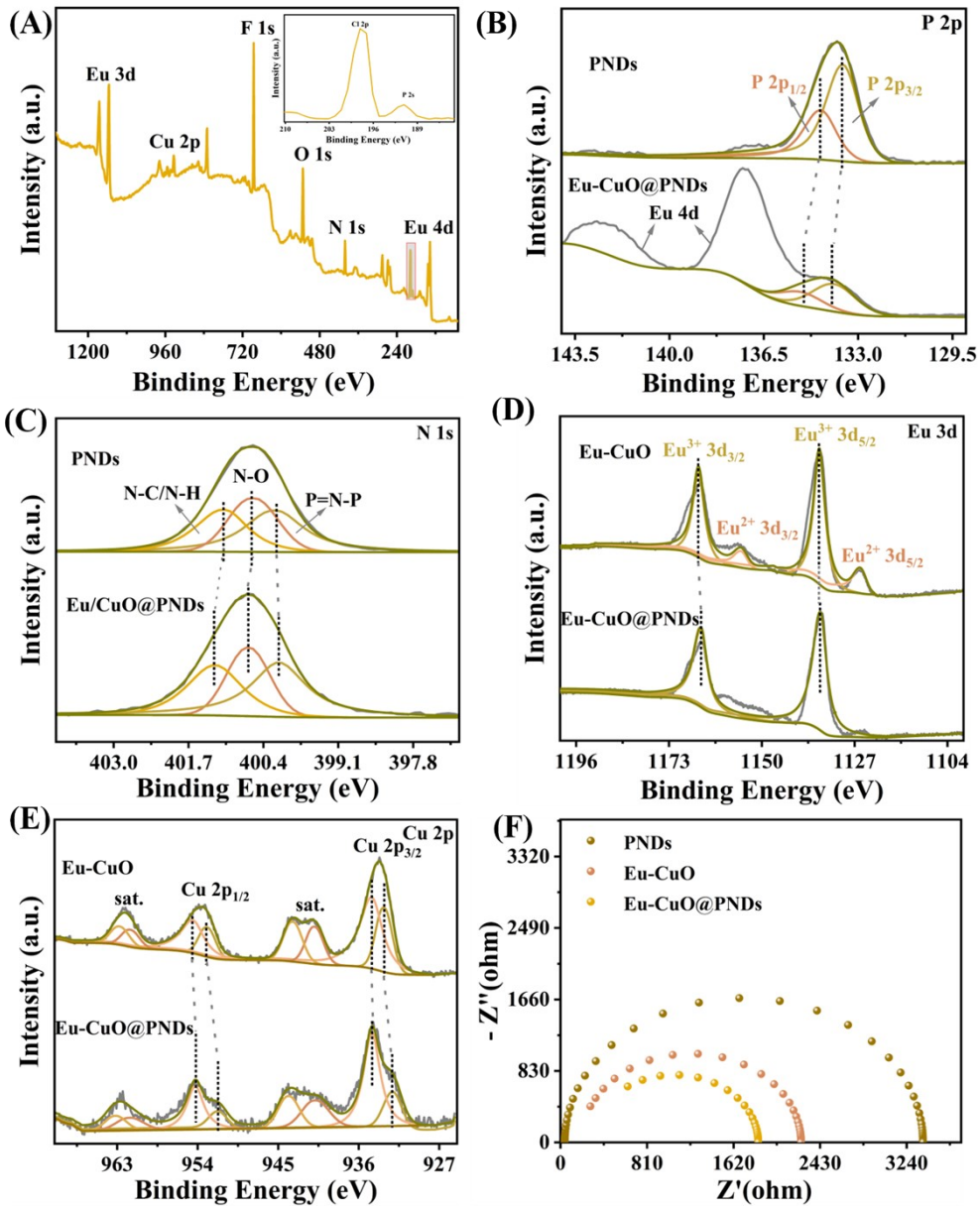

Figure S6. (A) Full XPS spectra of Eu-CuO@PNDs. High-resolution XPS spectra of (B) P 2p and (C) N 1s in PNDs and Eu-CuO@PNDs. High-resolution XPS spectra of (D) Cu 2p and (E) Eu 3d in Eu-CuO and Eu-CuO@PNDs. (F) EIS Nyquist plots of PNDs, Eu-CuO, and Eu-CuO@PNDs.

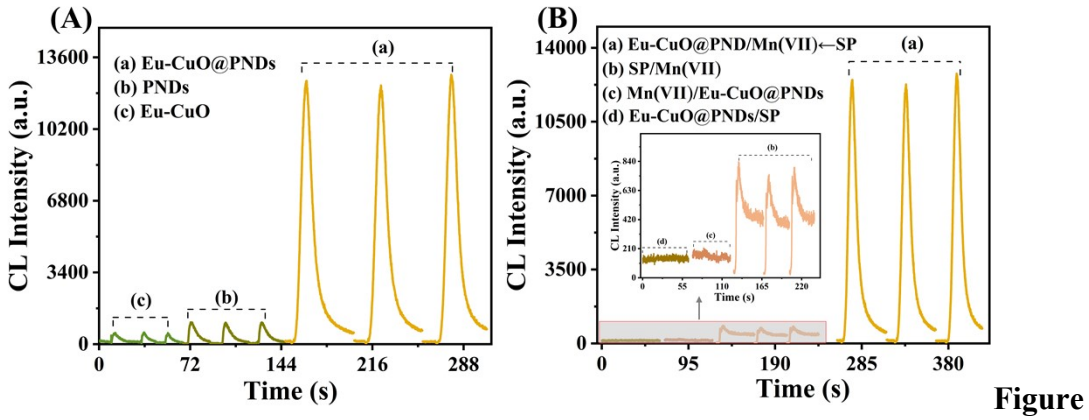

Figure S7. (A) CL intensity of Mn(VII)/SP system in the presence of (a) Eu-CuO@PNDs, (b) PNDs and (c) Eu-CuO. (B) CL intensity for (a) Eu-CuO@PNDs/Mn(VII)/SP, (b) SP/Mn(VII), (c) Mn(VII)/Eu-CuO@PNDs, and (d) Eu-CuO@PNDs/SP systems. (Experimental conditions: [Eu-CuO@PNDs]: 0.02 mg/mL; [PNDs]: 0.02 mg/mL; [Eu-CuO]: 0.02 mg/mL [Mn(VII)]: 1 mM; [SP]: 10 μg/mL.).

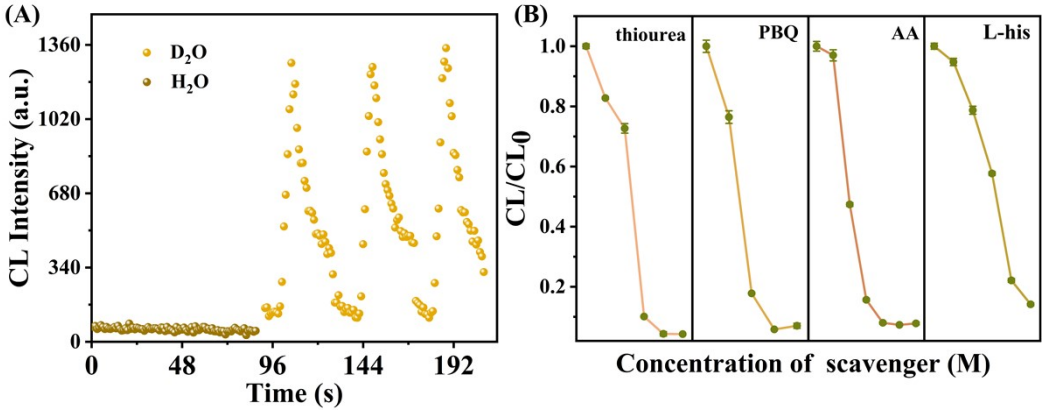

Figure S8. (A) CL intensity of Mn(VII)/Eu-CuO@PNDs system in D_2O or H_2O. (B) The inhibition percentage of scavengers on the CL for Eu-CuO@PNDs/Mn(VII)/SP system. (Experimental conditions: [Eu-CuO@PNDs]: 0.02 mg/mL; [Mn(VII)]: 1 mM; [SP]: 10 μg/mL.).

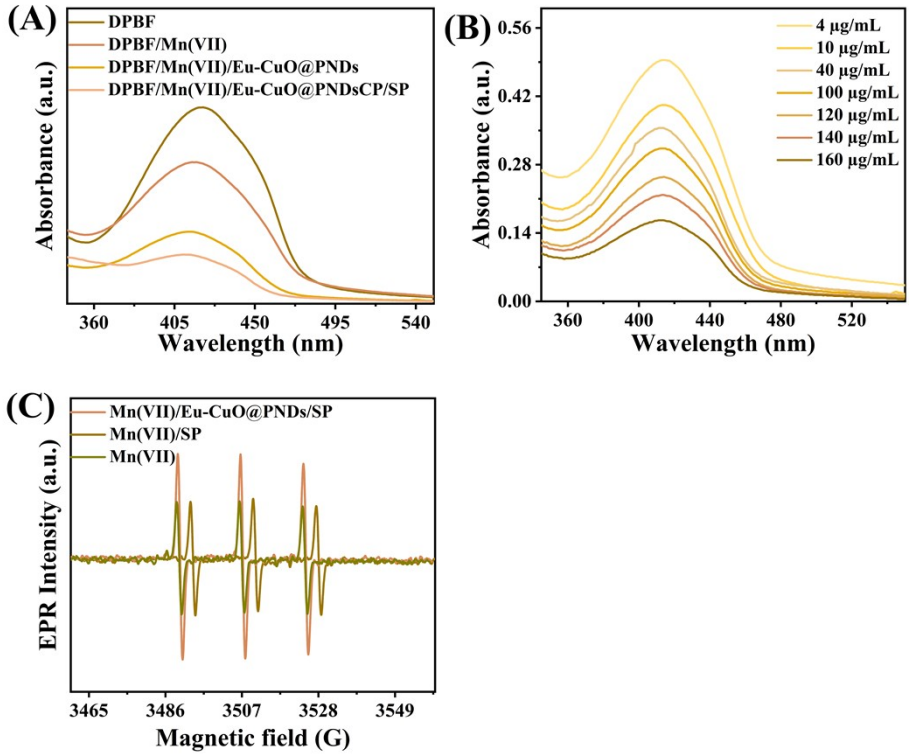

Figure S9. (A) UV-vis absorption spectra of DPBF for Mn(VII)/Eu-CuO@PNDs/SP system. (B) UV-vis absorption spectra of DPBF probe for different concentrations of Eu-CuO@PNDs in Mn(VII) solution. (C) TEMP-$^1O_2$ adduct EPR spectra for Mn(VII), Mn(VII)/SP and Eu-CuO@PNDs/Mn(VII)/SP systems. (Experimental conditions: [Eu-CuO/PNDs]: 0.02 mg/mL; [Mn(VII)]: 1 mM; [DPBF]: 0.005 mg/mL; [SP]: 10 μg/mL.).

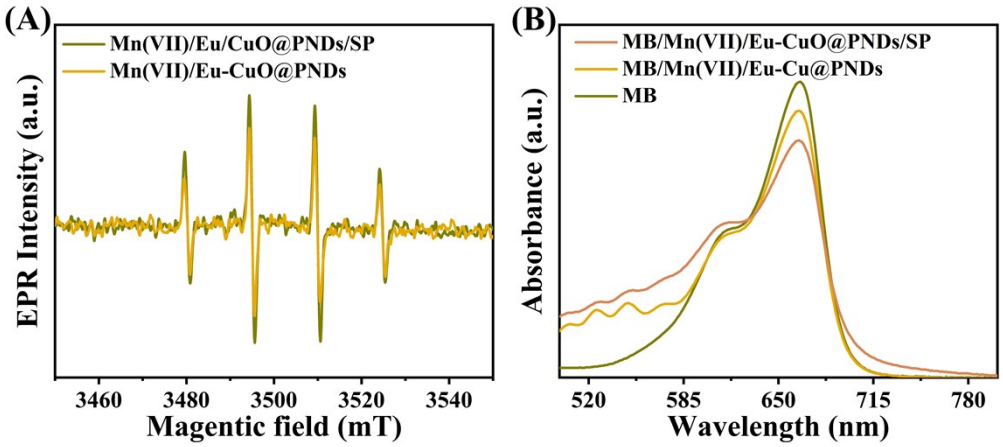

Figure S10. (A) DMPO-$^{\bullet}$OH adduct EPR spectra and (B) UV-vis absorption spectra of MB probe for Eu-CuO@PNDs/Mn(VII) and Eu-CuO@PNDs/Mn(VII)/SP systems.

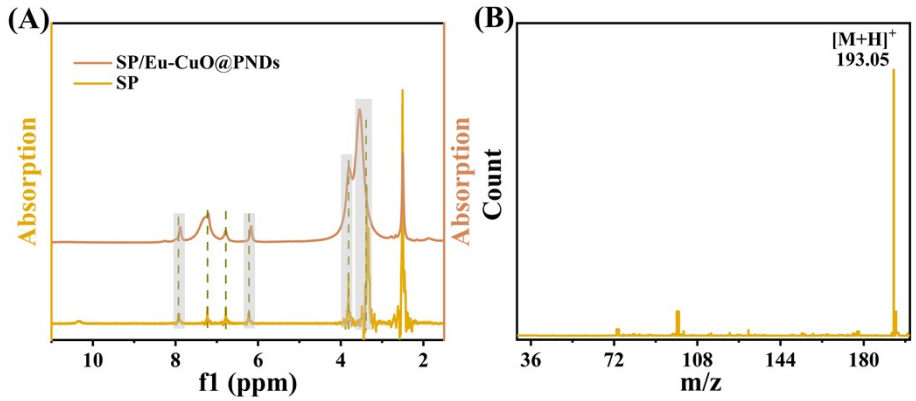

Figure S11. (A) ^{1}H NMR of SP and Eu-CuO@PNDs/SP system. (B) MS spectra of Eu-CuO@PNDs/SP system.

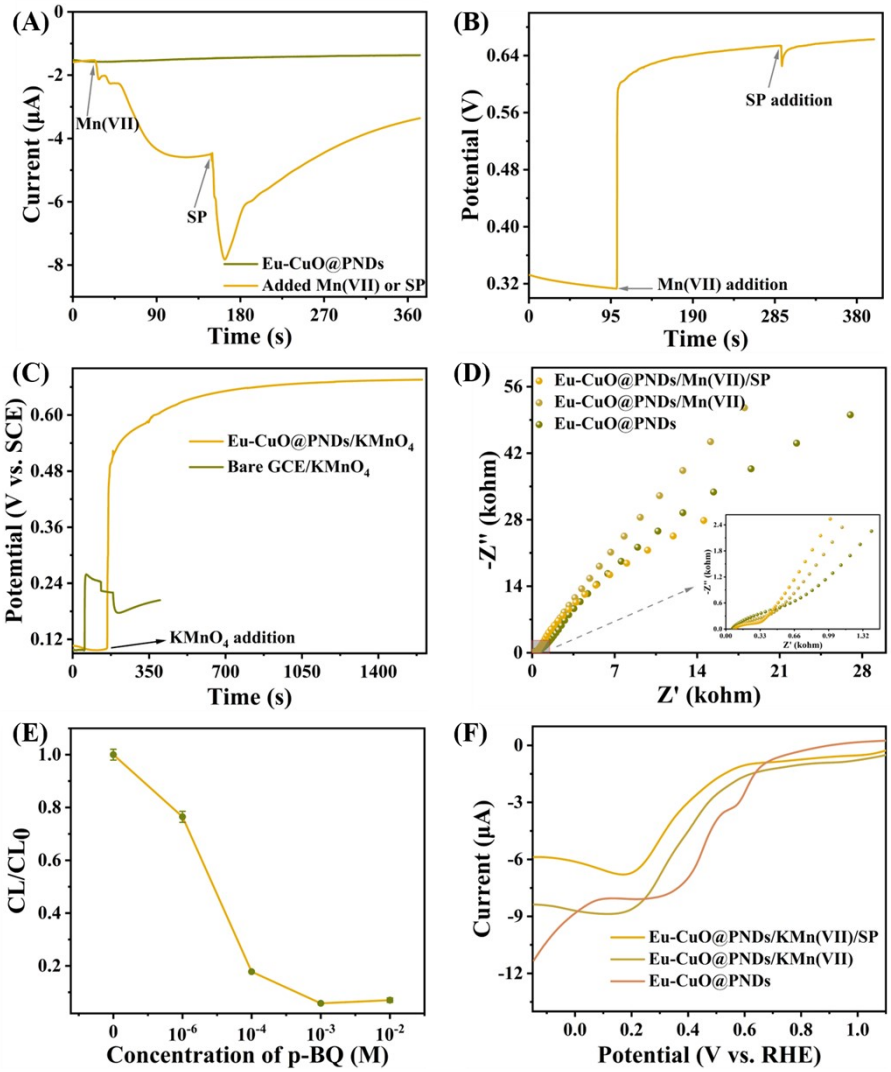

Figure S12. (A) Amperometric i-t curves and (B) OCP curve for Mn(VII)/SP system using Eu-CuO@PNDs as working electrode. (C) OCP curves for Mn(VII) solution using bare GCE or Eu-CuO@PNDs as working electrode. (D) EIS Nyquist plots for

Eu-CuO@PNDs/Mn(VII)/SP, Eu-CuO@PNDs/Mn(VII) and Eu-CuO@PNDs systems. (E) The effect of Ag^{+} on CL intensity for Eu-CuO@PNDs/Mn(VII)/SP system. (F) LSV curves for Eu-CuO@PNDs, Eu-CuO@PNDs/Mn(VII), Eu-CuO@PNDs/Mn(VII)/SP systems.

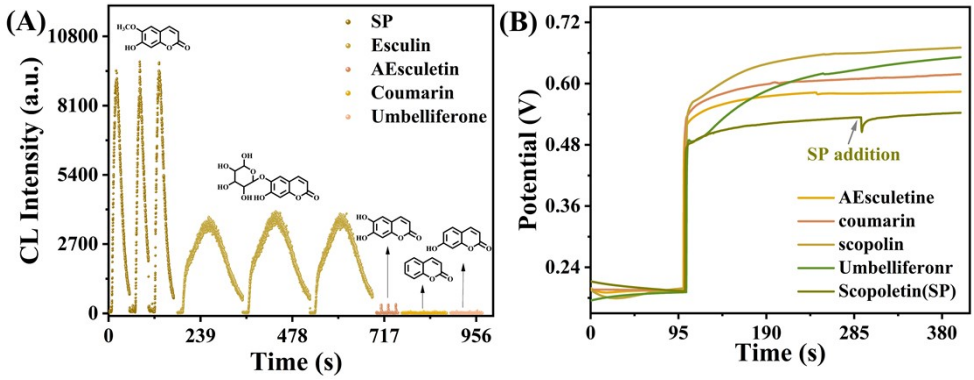

Figure S13. (A) CL intensity and (B-C) OCP curves of Mn(VII)/Eu-CuO@PNDs system toward other coumarin similarities to SP.

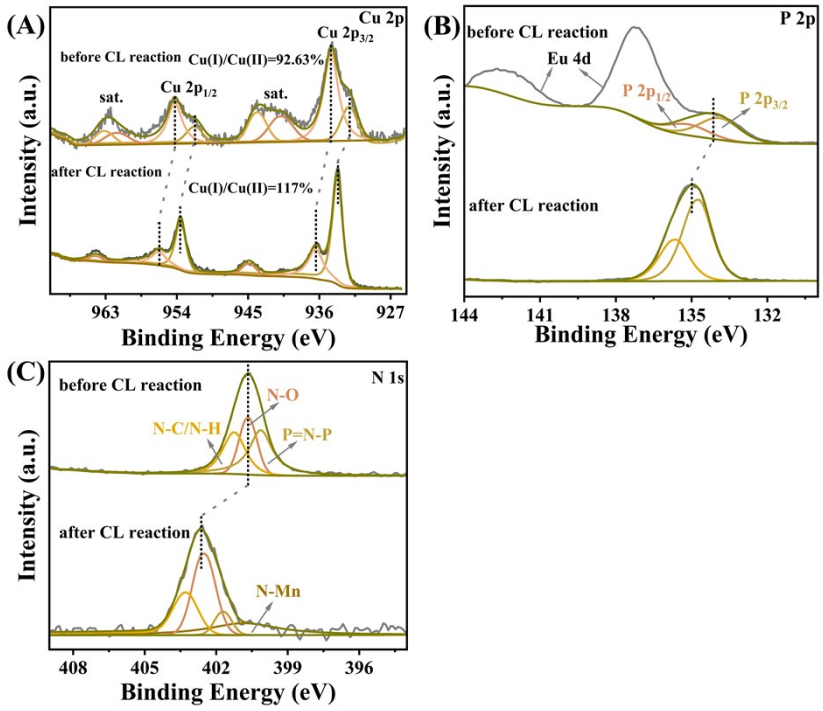

Figure S14. (A) Cu 2p, (B) P 2p and (C) N 1s high-resolution XPS spectra before and after CL reaction for Eu-CuO@PNDs.

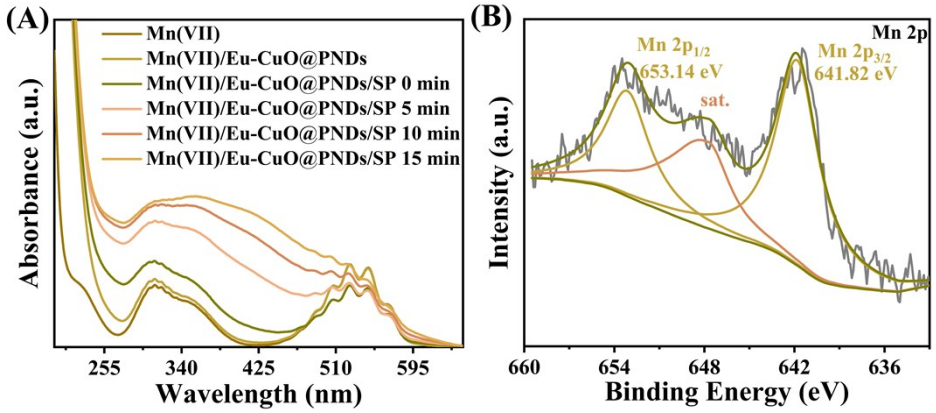

Figure S15. (A)The UV-vis spectra changes under different time for Mn(VII)/Eu-CuO@PNDs/SP system; (B) High-resolution XPS spectra of Mn 2p for Mn(VII) after CL reaction.

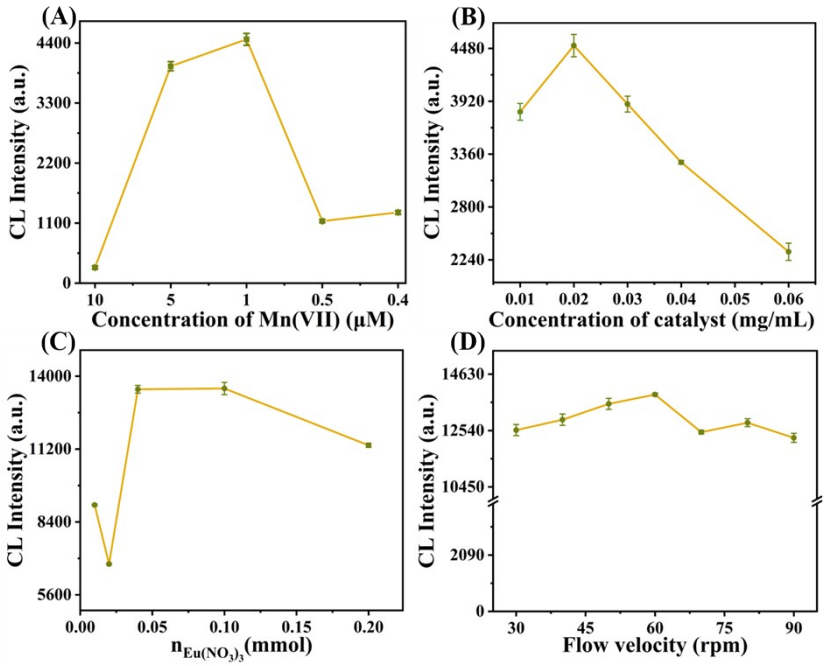

Figure S16. CL intensity under different Mn(VII) concentrations (A), Eu-CuO@PNDs concentrations (B), the amount of substance of $Eu(NO_3)_3$ (C) and flow velocity (D) for Eu-CuO@PNDs/Mn(VII)/SP system.

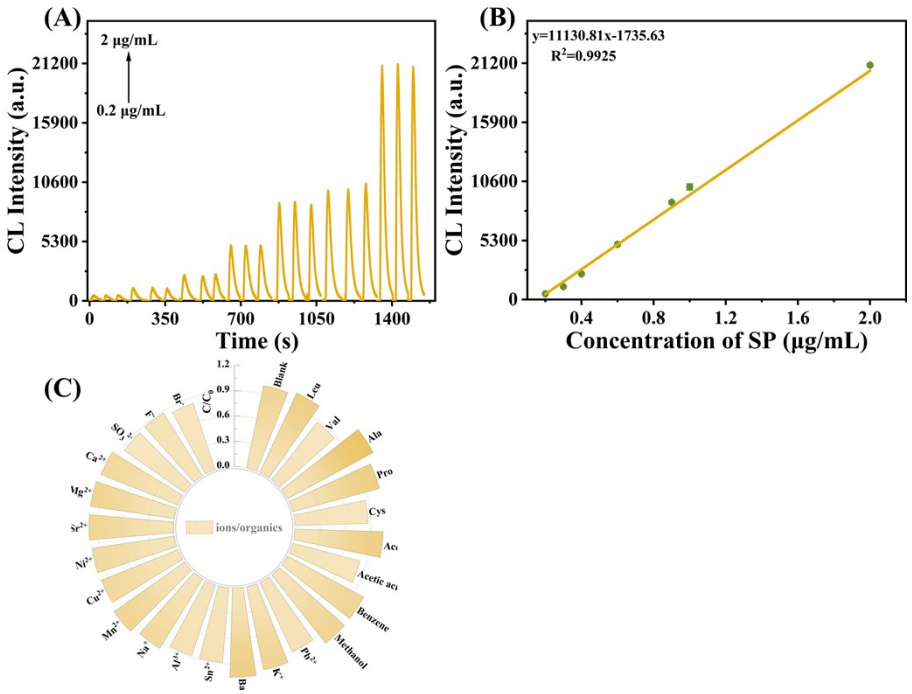

Figure S17. (A) CL kinetic curves of Eu-CuO@PNDs/Mn(VII) system with different concentrations of SP. (B) The linear relationship between CL intensity and SP concentration was from 0.2 to 2 μg/mL. (C) Anti-interference performance for Eu-CuO@PNDs/Mn(VII)/SP system in the presence of various interferences.

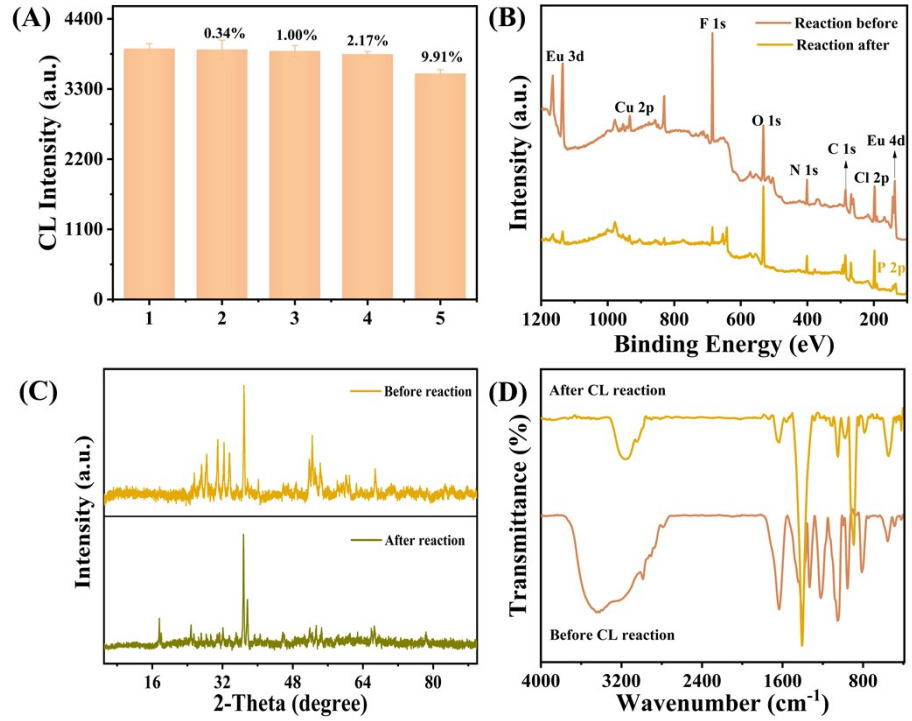

Figure S18. (A) The repeatability of the Eu-CuO@PNDs in the CL sensing system. (B) Full XPS spectra, (C) XRD spectra and (D) FT-IR spectra for Eu-CuO@CN before

and after the CL rection.

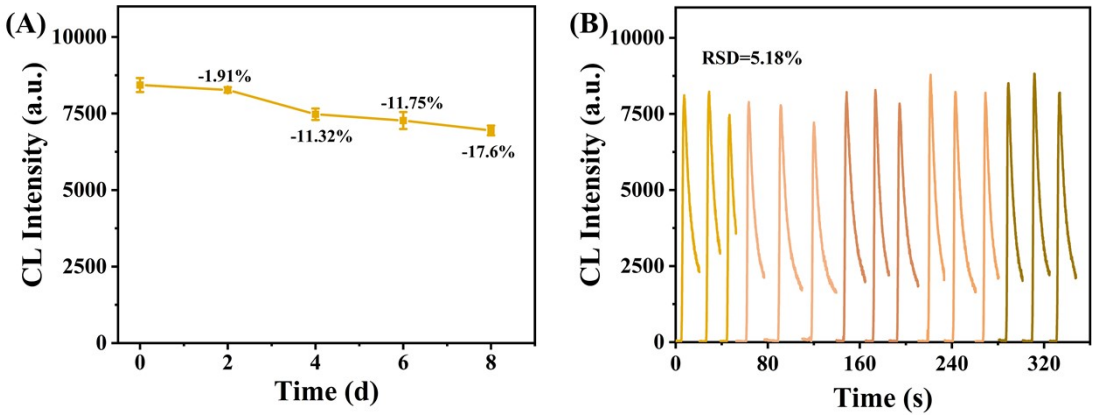

Figure S19. (A) The solution stability of the Eu-CuO@PNDs toward Mn(VII)/SP system and (B) repeatability properties of the CL sensing system. (Experimental conditions: [Eu-CuO@PNDs]: 0.02 mg/mL; [Mn(VII)]: 1 mM; [SP]: 1 μg/mL)

Table S1. Analytical performance comparison of SP determination methods.

Method	Linear range	LOD	Real samples	Reference
HPLC-UV	0.39-50 μg/mL	0.02 μg/mL	Eurycoma longifolia Jack and Eurycoma harmandiana Pierre	[4]
MALDI-HRMS	0.16-5 μM	0.04 μM	rabidopsis thaliana	[5]
Chemometrics-assisted excitation-emission matrix	0.25-2.5 mg/mL	-	Ercybe obtusifolia Benth	[6]
Electrochemical sensor	0.45 mM-2 mM	0.89 μM	Atractylodes macrocephala	[7]
qNMR	0.012-1.50 mg/mL	0.009 mg/mL	Paederia foetida	[8]
Chemiluminescence	0.2-2 μg/mL	0.018 μg/mL	wheat seed and Radix Codonopsis	This work

Table S2. Determination of SP concentration with the proposed CL method.

Sample	Spike (μg/mL)	CL Found (μg/mL)	Recovery (%)	RSD (%)
Wheat seed	0.35	0.36	102.86	3.00
	0.65	0.52	80.00	0.13
	0.95	0.99	104.21	1.47
	1.25	1.34	107.20	1.62
Radix Codonopsis	0.35	0.32	91.43	1.32
	0.65	0.53	81.54	1.25
	0.95	0.91	95.79	0.75
	1.25	1.09	87.2	1.47

Table S3. The conclusion of CL quantum yields, CL intensity and detection performance

CL system	CL quantum yields (E/mol)	CL intensity (a.u.)	Detection target	*LOD*	linear range	Reference
CPN PFV-co-MEHPV/ClO^-	2.51×10^{-5}	-	ClO^-	0.47 μM	2-30 μM	[9]
Si_3N_4 NPs-ClO^--diquat	1.02×10^{-4}	4500	diquat	6.1 μg/L	10-200 μg/L	[10]
DPKBH-TCPO-H_2O_2	4.59×10^{-10}	-	Pb^{2+}	0.45 mg/L	2.07-41.4 mg/L	[11]
Eu_2O_3/BPQDs-ClO^-	3.01×10^{-8}	6000	ClO^-	0.2×10^{-3} mM	0.001-1 mM	[12]
Eu-CuO@PNDs /Mn(II)/SP	3.12×10^{-9}	21200	SP	0.018 mg/L	0.2-2 μg/mL	This work

Note: 1. CPN PFV-co-MEHPV: Conjugated-polymer nanoparticles-Poly[(9,9-di(2-

ethylhexyl)-9H-fluorene-2,7-vinylene)-co-(1-methoxy-4-(2-ethylhexyloxy)-2,5-phenylenevinylene)]

2. DPKBH: fluorophores-di-2 pyridyl ketone benzoylhydrazone

3.TCPO: bis(2,4,6-trichlorophenyl) oxalate

References

[1] B. Zhu, W. Tang, Y. Ren and X. Duan, *Anal. Chem.*, 2018, **90**, 13714-13722.

[2] L. Li, C. Yu, F. Yang, C. Wang, K. Wei, K. Wang, X. Sun, L. Han and Y. Li, *Sep. Purif. Technol.*, 2025, **377**, 134326.

[3]. X. Wu, J. Shu, B. Feng, L. Yang, J. Lan, F. Li, P. Xi and F. Wang, *Chem. Commun.*, 2019, **55**, 4719-4722.

[4]. J. Chaingam, T. Juengwatanatrakul, G. Yusakul, T. Kanchanapoom and W. Putalun, *J. AOAC Int.*, 2021, **104**, 802-810.

[5]. L. Parasecolo, Ivan M. Monsalvo, N. Kovinich and Demian R. Ifa, *Rapid Commun. Mass Spectrom.*, 2024, **39**, e9973.

[6]. T. Liu, X.-G. Li, J.-Y. Wang, D.-L. Liu and Y.-J. Wei, *Spectrochim. Acta Part A*, 2019, **219**, 96-103.

[7]. Y. Yue, L. Zeng, X. Wang, L. Su, M. Sun, B. Wu and S. Yan, *Sci. Rep.*, 2019, **9**, 3864.

[8]. D. C. Tan, A. Quek, N. K. Kassim, I. S. Ismail and J. J. Lee, *Molecules*, 2020, **25**, 5162.

[9] B. Zhu, W. Tang, Y. Ren and X. Duan, *Anal. Chem.*, 2018, **90**, 13714-13722.

[10] D. Zhao, Y. Zhou, H. Gong, J. Gou, X. Xiao and H. Liu, *Sens. Actuators B Chem.*, 2023, **397**, 134525.

[11] L. C. de Paula Oliveira, I. Gaubeur and P. Dantoni, *J. Lumin.*, 2017, **183**, 418-423.

[12] H. Gong, D. Zhao, Y. Zhou, Y. Zhou, J. Gou and H. Liu, *Chem. Commun.*, 2023, **59**, 5110-5113.